SLANTED-AXIS ANTENNA DESIGN II

Jingquan Cheng
Sept. 14, 1993

ABSTRACT

The first part of the slanted-axis antenna design reports dealt with structural aspects of the antenna. This is the second part of the design reports. In this part of the reports, two aspects are discussed. These are the natural frequency and the thermal design. For the mmA antenna design, these two aspects place great challenges for design engineers as no existing astronomical antennas of such size can meet the fast switching as well as deformation requirements. In this report, the first chapter discusses the relationship between the structural parameters and natural frequency. It also discusses ways to increase the antenna natural frequency. In this chapter, a box-type backup structure is also discussed. The box-type antenna structure has a higher natural frequency and smaller surface deflection. In the second chapter,the antenna thermal problem is discussed. This report provides related data, formulae and definition on antenna thermal design. It also provides some results from Nastran heat transfer calculations. The backup structure deformation under thermal loading is also discussed with the help of Nastran program. However, detailed wind effect on the antenna is still excluded from this part of the reports.

CONTENTS

1. DISCUSSION ON NATURAL FREQUENCY OF ANTENNA STRUCTURE

1.1 Introduction

In the first part of the slanted-axis antenna design study, discussion on dynamic performance of the antenna structure was provided. The preliminary design of the antenna structure has a natural frequency of 9.72 Hz. However as indicated in section 4.5 of the previous report, in order to accommodate the fast switching phase calibration, a much higher structural natural frequency is desirable, although the requirement for natural frequency could be reduced if a higher damping coefficient is provided or a longer settling time and lower pointing accuracy are allowed. Increasing settling time and lowering the pointing accuracy are always undesirable to astronomers. Therefore, a question has to be answered here is: could the slanted-axis antenna been designed have an even higher natural frequency? In this and following sections, this and related problems are discussed.

Structure natural frequency is related to the structure response of external load. The general equation of a structure under an external load can be described as:

$$[M]\{\ddot{u}\} + [B]\{\dot{u}\} + [K]\{u\} = [F(t)]$$

where [M} is the mass matrix, [B] is the damping matrix, [K] is the stiffness matrix, [F(T)] is a time dependent load matrix and {u} is the vector of grid point displacements. In case of fast calibration switching or under wind, load [F(t)] will involve various components of different frequencies. The load can be represented by its spectral density $S_F(n)$. The corresponding spectral density of the response of the structure, $S_x(n)$, is[1]:

$$S_x(n)=H^2(n)S_F(n)$$

where H(n) is called mechanical magnification factor or mechanical admittance function. A large magnification factor for most structures is undesirable. The magnification factor of antenna structure is complex since the structure involves many vibration modes. For a single degree mass-spring system with a harmonic excitation $F(t) = F_0 \sin\omega_f t$[2],

$$H = 1 / [(1-r^2)^2 +(2r\xi)^2]^{1/2}$$

where r is the frequency ratio, $r = \omega_f / \omega$, ω is the structure natural frequency and ξ is the damping factor, $\xi = b /(2m\omega)$. The magnification factor calculated is shown in Figure 1. From the figure, the magnification factor will attain a higher value when the frequency ratio r is near to unity, which is called resonance. To avoid structural resonance, the struc-

ture natural frequencies should be kept away from the frequencies of the external excitation, which usually have a cut-off number at the high frequency end.

1.2 Vibration modes of the antenna structure

Any natural frequency of a structure is related to a particular vibration mode. Nastran analysis can provide for each mode its mode shape and the location in the structure where high strain will develop. From these analysis results, one can easily identify the weakest parts of the whole structure. After identifying these weakest parts, it is possible to stiffen the structure and to increase the natural frequencies of these particular modes. Nastran analysis of the preliminary design has been carried out. The first ten vibration modes of the preliminary design of the slanted-axis antenna, their mode shapes, their frequency values and locations of high strain, are listed in Table 1.

Table 1 Vibration modes of the slanted-axis antenna

mode	frequency(Hz)	description of mode shape	location of high strain
1	9.72	rotate around backup axis	backup structure
2	10.70	rotate in x-z plane	tripod
3	11.27	rotate in x-z plane	tripod
4	13.63	rotate in x-z plane	tripod and dish in opposite direction
5	13.92	wobbling in y-z direction	dish
6	17.54	up and down motion	tripod
7	18.66	dish wobbling in y-z direction	dish
8	21.02	dish wrapping in x-z plane	dish
9	21.03	dish wrapping in y-z plane	dish
10	21.50	rotating in x-z plane	dish

From Table 1, it can be found that these low vibration modes are all related to the dish structure and tripod structure. The frequencies of these two parts dominate the frequency of the whole antenna. They are very important when the resonance of the structure is concerned. However from the table, it can be found that some modes of the antenna have their vibration component perpendicular to the fast switching drive. These frequencies will have little effect on the structure resonance during the fast switching phase calibration. However, if wind or other excitation is concerned, these mode shapes may not be as important as the frequency values.

1.3 Natural frequency and antenna structure parameters

Since the natural frequency of the antenna is mainly determined by the dish and tripod structures. Therefore in this section only these two parts are discussed. The dish of the antenna(including backup truss and the panels) is a complex structure, the structure members involved are at different orientations and they may have different cross-section areas as well. The relationships between the structure parameters and the natural frequency are not straightforward. Therefore, it is necessary to simplify the structure in order to understand these relationships.

The vibrations of the dish structure can be divided into two groups; one is happened on the plane which is perpendicular to the dish axis and the other is on the dish axis planes. The vibration modes on the plane which is perpendicular to the dish axis concern the torsional stiffness of the dish and those on the axis planes concern the bending stiffness. The torsional stiffness of the dish is mainly provided by diagonal and 'V' shape members between radial rings. The torsional stiffness of these diagonal and 'V' shaped members provides reliable circumferential connection around the dish axis. The torsional stiffness of the dish is then transfered via these members from the center towards the edge. Therefore, every ring of these 'V' shaped members should have similar rigidity so that the dish can maintain a certain level of the vibration frequency. The 'V' shaped truss structure has been discussed in the Appendix of the previous design study. Their torsional natural frequency is:

$$\omega = (1/2\pi)(K / J)^{1/2}$$

$$K = 2\, n(R_2 \sin (\pi/n))^2 R_1^2 AE/L^2$$

where K is the torsional stiffness, J is the moment of inertia, R_1 is the supported ring radius and R_2 is the base ring radius, n is the number of repeated 'V' shape trusses in the whole circle, L is the truss member length, A is the trusses cross section area and E is Young's modulus. To estimating the frequency, taking J = 15,000 kg-m (for a dish with its mean mass radius of 2 m, and its total mass of 3750 kg), L = 2.5 m, R_1= 2 m, R_2 =1.5 m, n =12, A= 2.14x10 m^2(for a 25 mm diameter tube with tube wall thickness of 3 mm) and E = 1.27×10^{11} N/m^2(for CFRP material), then, the frequency estimated is ω = 10.3 Hz. This estimation agrees very well with the Nastran analysis of the preliminary design(see mode 1 of Table 1).

Concerning the vibration modes which are on the dish axis planes, a plate analogy approach is developed. For an isotropic plate, its bending stiffness, D, is expressed as:

$$D = h^3 E/[12(1- \nu^2)]$$

where h is the plate thickness and ν is poisson's ratio and E is young's modulus. Since the antenna dish structure is a truss structure and not a simple plate, this formula is difficult to

be applied. However as a double layer truss structure, the plate analogy can be applied. The equivalent bending stiffness for a double layer truss structures had been derived by Makowski. If the member cross section areas are the same for a double layer trusses then the equivalent bending stiffness of it is expressed as[3]:

$$D = A h^2 E/(2b)$$

where A is the cross section area of the truss members, h is the truss height, b is the separation between top members and that between bottom members and E is Young's modulus. With this approximation, the dish can be replaced by a simple plate which has approximately the same bending stiffness as the dish. By substituting the bending stiffness to the following formula of vibration frequency for a circlar plate which is supported at a middle ring which has a radius 0.4 times of the plate outer radius, the dish vibration frequency can be calculated. The formula of the plate natural frequency under the mentioned condition is[4]:

$$\omega = (6.7/2\pi a^2)[D/\rho]^{1/2}$$

where a is the outer radius of the plate, D is the bending stiffness and ρ is the density of the plate per unit area. By taking the data of the slanted-axis antenna dish, a= 4 m, A = 2.14×10^{-4} m^2(25 mm diameter tube), h = 0.6 m(average truss height), b = 0.8 m(average surface beam seperation) and ρ = 60 kg/m^2 (including the mass of panels and truss members), then the frequency calculated is 16.3 Hz. This also agrees well with the Nastran analysis results(refer to modes 5 and 7 of Table 1).

The natural frequency of the tripod structure has been discussed in the appendix of the previous report. The same formula as the torsional natural frequency of the dish structure can be used, but the individual values of the parameters are different. The tripod in the preliminary design has a larger radius ratio between its supporting and supported rings, and a long truss member length so that the natural frequency of the tripod structure is low. In the slanted-axis design, the tripod may be a dominant factor in limiting the antenna natural frequency.

1.4 Ways to increase natural frequency of the dish and tripod structures

In the previous section, approximate formulae have been provided to estimate the natural frequency of the dish and tripod structure when they vibrate in different mode shapes. From these formulae, it can found that the natural frequency of the dish and the tripod for all the modes is proportional to the $(AE)^{1/2}$, and is also inversely proportional to the structure mass or the structure mass density. Increasing the member cross section area will increase the natural frequency of the same vibration mode at a rate of the square root if the mass increase is not significant(for CFRP members used in the dish structure, this statement could be true as the panel and joint nodes are main structure mass, but it will not be

true if it is applied to the tripod structure). Therefore we always can increase the dish structure natural frequency by using structure members with a larger cross section area. However, it will be difficult to improve the natural frequency of the tripod by simply increasing its member cross section areas. By changing the radius ratio of supporting and supported rings or by shortening the member length, the natural frequency of the tripod could be increased. Another point which could be drawn from the natural frequency formulae is that the natural frequency of a dish structure is inversely proportional to the square of its outer radius. The larger the dish diameter is, the lower the natural frequency will be. If two dishs have a similar design, a 6 m diameter antenna will have its natural frequency 1.77 higher than a 8 m diameter one.

For checking the above approximate formulae, Nastran analysis has been performed by changing all the members which have their diameter of 25 mm to memberes of 32 mm diameter in the dish structure, the rest of members are remained unchanged. In this way, the cross section area of these members then increases from 2.14×10^{-4} m^2 to 2.74×10^{-4} m^2. The calculated natural frequency of the whole antenna from Nastran analysis is now 10.23 Hz instead of 9.72 Hz. The frequency ratio of increase is 1.05. The square root ratio of the member cross section area is 1.13. This result agrees fairly well to the prediction. Small descrepancy in the result is caused by the mass increase and those unchanged structure members. The new antenna now weighs 21,420 kg instead of 21,360 kg. In table 2, the main truss member size, their cross section area, area ratios and estimated frequency gain on the dish vibration modes are listed. However, when the dish structure is stiffened, the primary vibration mode may shift to other parts of the antenna.

Table 2 Antenna natural frequency and truss member size

Tube size	section area	area ratio	square of ratio	frequency gain*
25 mm	214 mm^2	1	1	1
32 mm	274 mm^2	1.28	1.13	1.05
38 mm	639 mm^2	2.98	1.75	1.20
50 mm	892 mm^2	4.16	2.04	1.30

* these are estimated frequency gain.

Tripod structure vibration mode is a dominant factor which lowers the natural frequency of the whole antenna. Analysis in the previous report has shown that the natural frequency of a tripod is higher compared with other types secondary mirror support with eight or more truss members. Besides the member cross section area, from the previous formula the natural frequency of the tripod structure is also related to the radius ratio of its top and bottom rings. It is also inversely proportional to the length of the tripod members. In the previous design, the top ring has a triangular shape. The radius ratio of the top and bottom support rings is large. To improve this situation, a modification of the tripod is developed

true if it is applied to the tripod structure). Therefore we always can increase the dish structure natural frequency by using structure members with a larger cross section area. However, it will be difficult to improve the natural frequency of the tripod by simply increasing its member cross section areas. By changing the radius ratio of supporting and supported rings or by shortening the member length, the natural frequency of the tripod could be increased. Another point which could be drawn from the natural frequency formulae is that the natural frequency of a dish structure is inversely proportional to the square of its outer radius. The larger the dish diameter is, the lower the natural frequency will be. If two dishs have a similar design, a 6 m diameter antenna will have its natural frequency 1.77 higher than a 8 m diameter one.

For checking the above approximate formulae, Nastran analysis has been performed by changing all the members which have their diameter of 25 mm to memberes of 32 mm diameter in the dish structure, the rest of members are remained unchanged. In this way, the cross section area of these members then increases from 2.14×10^{-4} m^2 to 2.74×10^{-4} m^2. The calculated natural frequency of the whole antenna from Nastran analysis is now 10.23 Hz instead of 9.72 Hz. The frequency ratio of increase is 1.05. The square root ratio of the member cross section area is 1.13. This result agrees fairly well to the prediction. Small descrepancy in the result is caused by the mass increase and those unchanged structure members. The new antenna now weighs 21,420 kg instead of 21,360 kg. In table 2, the main truss member size, their cross section area, area ratios and estimated frequency gain on the dish vibration modes are listed. However, when the dish structure is stiffened, the primary vibration mode may shift to other parts of the antenna.

Table 2 Antenna natural frequency and truss member size

Tube size	section area	area ratio	square of ratio	frequency gain*
25 mm	214 mm^2	1	1	1
32 mm	274 mm^2	1.28	1.13	1.05
38 mm	639 mm^2	2.98	1.75	1.20
50 mm	892 mm^2	4.16	2.04	1.30

* these are estimated frequency gain.

Tripod structure vibration mode is a dominant factor which lowers the natural frequency of the whole antenna. Analysis in the previous report has shown that the natural frequency of a tripod is higher compared with other types secondary mirror support with eight or more truss members. Besides the member cross section area, from the previous formula the natural frequency of the tripod structure is also related to the radius ratio of its top and bottom rings. It is also inversely proportional to the length of the tripod members. In the previous design, the top ring has a triangular shape. The radius ratio of the top and bottom support rings is large. To improve this situation, a modification of the tripod is developed

which is shown in Figure 2. In the new design, a hexagonal shaped top end replaces the triangular one. Therefore the new supported top ring has a larger radius. The natural frequency of this new structure is then increased. Further improvement of the tripod natural frequency can be made by increasing the tripod member stiffness. Using plane trusses to replace supporting members is one way of which many large antennas did. For significant improvement in the tripod natural frequency it is necessary to reduce the length of the tripod members by directly connecting the tripod to the backup structure. This approach is possible but needs more analysis and optimization. For stiffer backup structures such as the box-type ones, the optimization is easier. In this way, the natural frequency of the tripod and the whole antenna will be improved greatly. The discussion of the box-type backup structure will be in the following section.

1.5 Discussion on box-type backup structures

Most radio antennas have their backup structures made of tubular members. However there are few antennas having their backup structures made from thin wall box structures. In the astronomical field, antennas which have box-type backup structures are made by ESSCO. These backup structures use aluminum thin-walled boxes to form radial and circumferential ribs. This kind of arrangement provides high stiffness in both zenith and horizon directions. The antenna with this kind structure can be designed without using the homology approach. However the local buckling of these boxes is a problem. For avoiding that, many stiffening ribs have been added to stiffen the thin wall plates. The disadvantage of the ESSCO antenna is its resistance against strong wind. Also, the antenna is weak in torsional direction. Since ESSCO provides antennas for indoor use only, all these antennas have to be protected by ESSCO made radomes. Figure 3 shows a 13.7 m ESSCO antenna structure.

For ensuring the rigidity of the backup structure in all directions, the box element should have either a fan or a hexagonal shape as shown in Figures 4 and 5. Large opening on the box structure also helps to reduce the drag force due to strong wind. Composite Optics, Inc. (COI) developed a mortise-and-tenon box structure made by CFRP flat sheets(Figure 6). All these concepts have the same basic characteristics. They are more stiff than truss structure; they are light in weight since no joint nodes are required and they are easier in assembly and may be cheap in mass production. The hexagonal segment structure can be made from uniform elements and the resulting backup structure has a spherical surface shape. The fan shaped one could be built by three box rings. Its middle ring forms the main structure, and the inner and outer ring could be adjusted to the deflection requirement. This arrangement might be easier in the homology optimization. The Composite Optics concept is a combination of the truss structure and box structure. It may cost less since it involves minimum manual labor in the production. Also its surface deflection may be optimized by dividing the whole structure into many 'I' beams, but the effect of epoxy material in the plate connection needs more attention. In summary, all these concepts have difficulties in the structure analysis because they require more elements and more grid points. For estimating the performance of the box-type backup structure, a analogy formula could be used

again. The approximation of the bending stiffness[5] of a box type structure is:

$$D = E I / b$$

where E is the Young's modulus, I is the moment of inertia of a single element and the b is the distance between repeated box elements. Taking a rough estimation, if the box element has a dimension of 0.8x0.8x0.6 m(0.6 m is its height) and the box wall thickness is 0.005 m, then its bending stiffness for CFRP is 1.28×10^8, this is about 20 times of that of a truss type structure if it is made by 25 mm diameter CFRP tubes with the same separation and height(the bending stiffness is about 6.1×10^6). Therefore, the deflection of this backup structure is also much smaller than that of the truss type structure. In the same time, heavy node joints for the truss structure are eliminated. Nastran analysis results confirmed this statement. The analysis results will be presented in the following section. The dish natural frequency will also increase significantly. Since the dish has a higher bending stiffness, the tripod could be directly connected to the backup structure so the natural frequency of the tripod can be improved.

In summary the advantages of using a box-type backup structure are:

* the rigidity of the structure is increased; the deflection is lower and the natural frequency is higher;
* the tripod could be connected to the backup structure directly; its natural frequency is therefore increased;
* due to the reduced dish weight, the overall weight of the antenna can be reduced significantly;
* eliminate the joint nodes which is heavy and thermally undesirable;
* simplify the assembly process, saving the assembly time and labor;
* in case of mass production, the cost of the structure might be lower.

The disadvantages of using box-type backup structure are:

* accurate modelling and analyzing are difficult;
* the surface support points may not fit very well to a new parabola and optimization of the structure is different;
* detailed structure design to avoiding any possible local buckling under extreme load condition is required;
* the manufacture of CFRP boxes is complex and labor intensive; a prototype structure could be expensive.

1.6 Nastran analysis of box type antenna structure

The dynamic advantage of a box type structure has been discussed. For assessing the static performance of the box type structure, simple models have been produced. Figure 7 shows a section of a very rough box type structure model. In this model, the shape of the support ribs are arbitrarily determined for the purpose of the analysis, it has not optimized. The load on the surface support points is the same as those of the models we used before by assuming it comes from 20 kg/m^2 aluminum panels. The plates of the structure are 8 mm thick CFRP ones. There are three circumferential stiffening ribs rings and twelve radial ribs. The analysis of this simple model gives the deflection pattern of the surface nodes. Figure 8 shows the deflection pattern. From the figure, it can be found that the deflection is only 12 microns. So it is not necessary to do much optimization or homological fitting.. For this type of structure, the tripod weight will bring very small dent in the reflecting surface. The overall natural frequency will be increased.

Calculations have also been performed for the COI type structure, which is easier than that mensioned above. By substituting I-beam parameters into the tube ones in the truss structure, the structure can be easily analyzed. We choose the the I-beam height to be 50 mm, the top and bottom width 25 mm and the thickness 3 mm and we replace only the 25 mm tubes by this type of I-beams in the backup structure and the rest of the structure members remain unchanged. The analysis results of the new COI structure shows that the largest absolute deflection of the dish surface nodes has been reduced from 298 microns to 106 microns, and the backup structure weight is also reduced from 3685 kg to 2297 kg. In the scaled model provided by COI, the thickness of the members is only 1.15 mm thick. Using this thickness to form new I-beams, the stiffness of the structure will be higher again and the deflections of the structure will be smaller. For COI or similar structures, the absolute deflection is still larger than that allowed, so fitting to a new parabola is still necessary. Of course, as mention already, the local buckling remains a structural problem needing further study.

1.7 Wind energy spectrum

The wind is another source for the antenna vibration besides the fast calibration switching. Wind contains a wide range of excitation frequencies. The general trend for the wind excitation is that as the main wind speed increases, the peak energy of excitation increases and moves to high frequency. The wind energy spectrum S(n) is a function of frequency (n) and mean speed (V). Davenport derived an empirical formula[6] as:

$$S(n) = [\, k\, V^2 / n \,]\, [\, 4\, u^2 / (1 + u^2)^{4/3} \,]$$

where u = 1200 n/V, n is frequency in unit of Hz, V is the velocity in the unit of m/sec measured at a standard height of 10 m above ground in the unit of m/sec, k is the coefficient related to the ground smoothness, varying from 0.0005 for sea surface to 0.05 for rough ground. The wind energy spectra for a rough surface when the wind speed is 20 m/sec and 60 m/sec are shown in Figure 9. From the figure, it can be found that most of the wind

energy falls in the range below 1 Hz. These frequency ranges are far away from the antenna natural frequency we attempt to achieve. Therefore the dynamic effect of wind is small for this mmA antenna design.

2. DISCUSSION ON ANTENNA THERMAL DESIGN

2.1 Antenna thermal conditions

For an open-air structure, the future mmA antenna will interact thermally with the ambient air, the sky, the ground and the sun. Inside the antenna structure, there are also some heat sources due to instrument power dissipation. All these determine the temperature distribution within the antenna structure. However, these conditions, especially the ambient thermal conditions, are all variables which are not possible to predict exactly. The random phenomenon of thermal problem makes the analysis difficult. However, with the help from some programs, thermal analysis is still possible. Lamb[10] did detailed study on the thermal performance of the mmA antenna, the reader can refer to mmA antanna Memo. No. 5.

Ambient air temperature T_A is a variable of the time t according to seasons or day and night. It can be treated as an infinite heat reservoir. The approximate pattern of T_A can be described by[7]:

$$T_A(t) = T_{A0} - \delta T_A \cos [\omega (t - t_0)]$$

where $\omega = 2 \pi / 24$ h, $T_{A0} = < T_A(t) >$ the daily average temperature, δT_A is the amplitude of the daily temperature variation and t_0 is the time delay of the variation with respect to 12 hour noon. t_0 is the order of 1 to 2 hours. The ambient temperature range is;

Temperature range 1	-15 to +25 C
Temperature range 2	-20 to +30 C

and daily variation of the temperature is about 10 C.

The sky, linked with the antenna by radiation, is also an infinite heat reservoir. The temperature of a clear sky can be represent by Swinbank's formula:

$$T_S(t) = 0.0553\ T_A(t)^{1.5}$$

The sky temperature can also be represented as:

$$T_S(t) = T_A(t) - \delta T_S$$

where $\delta T_S \sim 15 - 20$ C. The sky temperature depends on the water vapor contents which varies in time and place. When the antenna surfaces are radiatively coupled to the sky, the wavelengths are in the infrared range between 8 and 13 microns.

The ground temperature can also be represented as:

$$T_G(t) = T_{G0} - \delta T_G \cos[\omega(t - t_g)]$$

where $T_{G0} = < T_G(t)>$ the daily average ground temperature. δT_G is the amplitude of the temperature variation and t_g is the time delay of the variation with respect to 12 h noon. t_g is the order of 1-2 h. T_G can also be represented by the ambient temperature as:

$$T_G(t) = T_A(t) + \delta T_G$$

The radiation properties of the ground depend on the composition of the ground.

Solar loading is the major source of energy to the antenna structure. The amount of the irradiation varies from time to time and disturbs the thermal state of the antenna. Without the absorption from the earth's atmosphere, the maximum and minimum values of the total solar irradiance is 1420 W/m^2 for perihelion and 1288 W/m^2 for aphelion[8]. Data have been collected for the solar radiation at Mt. Whitney, which has an altitude of 4350 m. The measured nominal data is 1199 W/m^2. By using this data, it is expected that the solar radiation on a high altitude site will be 1260 W/m^2 for perihelion and 1140 W/m^2. Therefore, in this report, the data used for solar loading is as:

Solar loading 1260 W / m^2

The variation of the elevation angle $\beta(t)$ of the sun is calculated from:

$$\sin \beta(t) = \cos H(t) \cos \phi \cos \delta(E) + \sin \phi \sin \delta(t)$$

where H(t) is the hour angle, ϕ is the geographic latitude, and $\delta(t)$ is the declination of the sun for the epoch E.

Due to the variation of the solar elevation angle, the radiation of the sun received will be modified according to the equivalent air mass. The equivalent air mass (EAM) at an altitude is:

$$EAM = - (R/H) \cos \beta + \{ [(R/H) \cos \beta]^2 + 2 (R/H) + 1.0 \}^{1/2}$$

where R is the radius of the earth at the altitude(6378 km + altitude) and H is the thickness of unit air mass at the altitude(7,655 m for 4,100 m altitude). The calculated EAM is shown in Table 3.

Table 3 EAM as a function of elevation angle for a high altitude site

0	10	15	20	30	40	45	50	60	70	75	80	85	90
1.0	1.015	1.035	1.064	1.154	1.305	1.413	1.554	1.996	2.911	3.832	5.652	10.694	40.846

2.2 Formulae for heat transfer

Heat transfer generally includes three distinct modes: conduction, radiation and convection. Among all three modes, convection is most complicated since it involves mass transfer process.

For conduction, the rate of heat transfer is determined by the following formula[9]:

$$q_c = - k A \, dT/dx$$

where k is thermal conductivity, A is the conducting area, T(x) is the local temperature and x is the distance in the direction of the heat flow.

For radiation, the total power emitted by a gray body of temperature T is given by Stefan-Boltzmann law:

$$q_r = \sigma e A T^4$$

where $\sigma = 5.67 \times 10^{-8}$ W/m^{2}K is the Stefan-Boltzmann constant, e is the emissivity of the surface and A is the area. The heat transfer between two grey bodies is determined by the temperature difference, their emissivities, their absorptivities, their surface areas and their relative position.

Heat transfer by convection can be expressed in general as:

$$q_{cv} = h_{cv} A (T_s - T_a)$$

where h_{cv} is the convection coefficient, A is the area, T_s is the surface temperature and T_a is the air temperature. However, the convection coefficient h_{cv} which may vary over the surface depends on many factors: such as air density, viscosity, velocity and thermal

properties. Higher wind speed will greatly help the heat convection and result in smaller temperature gradients between exposed components. However, natural convection will have a smaller convection coefficient and may cause a temperature gradient which is undesirable for the antenna structure. For evaluating the heat transfer by convection, related formulae are listed below.

a) Dimensionless number formulae

Reynolds number $Re = U_\infty L / \nu$

Prandtl number $Pr = \nu / \alpha$

Grashof number $Gr = g \beta (T - T_\infty) L^3 / \nu^2$

where U_∞ is a characteristic velocity, L is a characteristic length, g acceleration due to gravity, β is the expansion coefficient, $T-T_\infty$ is temperature difference, ν is the viscosity and α is thermal diffusivity.

b) formulae for horizontal plate

Average convection coefficient h_{cv} is related to the average Nusselt number Nu by:

$$Nu = h_{cv} L / k$$

where L is the dimension of the object, k is thermal conductivity.

When the plate is facing upward, Nu is:

$$Nu = 0.16(Gr\ Pr)^{1/3} \qquad \text{for } 7\times10^6 < Gr\ Pr < 2\times10^8$$

$$Nu = 0.13(GR\ Pr)^{1/3} \qquad \text{for } 5\times10^8 < Gr\ Pr$$

where Gr is Gashof number, Pr is Prandtl number, Pr = 0.71 for air.

when the plate is facing downward, Nu is:

$$Nu = 0.58(Gr\ Pr)^{1/5} \qquad \text{for } 10^6 < Gr\ Pr < 10^{11}$$

c) formula for a horizontal positioned tube convected through outer surface:

$$Nu = 0.53 (Gr\ Pr)^{1/4}$$

In many cases, a thermal time constant is used for evaluating the time required for elements to reach the environment temperature when a temperature difference exists between a component and its environment. One formula for the thermal time constant dealing with conduction is[10]:

$$T = \rho\ c_p\ L^2/(4k)$$

where ρ is the density, c_p is specific heat, L is the characteristic length and k is the conductivity. For convection, the formula of time constant is:

$$T = \rho c_p\ L/h$$

where h is the rate of heat transfer.

2.3 Basic data for thermal design

Thermal property data are different between different sources. Some of these data are not always available. In this report the mentioned data are from some related references.

Table 4 is the thermal properties of some structural materials and Table 5 is the properties of air at atmospheric pressure which is important in calculating the coefficient in natural or forced convections.

For structure members directly under the sun the absorption coefficient may differ from their emissivity, since their body temperature is around 293 K. These two numbers for some materials may not be the same. Table 6 listed some data for related surface materials[11].

Table 4 Thermal properties of some structural materials

Material	Density kg / m3	Specific heat J / (kg C)	Thermal expansion $x10^{-6}$ (1/ C)	Conductivity W/ (m C)
Carbon steel	7800	418	12.7	52
Aluminum	2700	962	23.0	156
CFRP	1600	710	0-4	4.2

* from Table 2 of mmA antenna memo No. 5 by J. Lamb[10].

Table 5 Thermal properties of dry air at atmospheric pressure

Temperature T (°C)	Density ρ (kg/m^3)	Thermal expansion $\beta x10^3$ (1/K)	Specific heat C_p (J/kg K)	Thermal conductivity κ (W/m K)	Thermal diffusivity $\alpha x10^6$ (m^2/S)	Kinematic viscosity $\nu x10^6$(m^2/s)
0.	1.252	3.66	1011	0.0237	19.2	13.9
20.	1.164	3.41	1012	0.0251	22.0	15.7
40.	1.092	3.19	1014	0.0265	24.8	17.6
60.	1.025	3.00	1017	0.0279	27.6	19.4

* from Table 27 of Appendixes of Principles of heat transfer by F. Kreith and M.S. Bohn.

Table 6 Absorptivity and emissivity of some surface materials

material	surface	absorptivity	emissivity
Gold	polished	0.01-0.07	0.01-0.07
Aluminum	polished	0.04-0.06	0.04- 0.06
	rough	0.07	0.07
	oxidized	0.2-0.33	0.2-0.33
TiO_2 paint		0.15-0.3	0.8
Graphite		0.81-0.9	0.81-0.9

2.4 Dish temperature distribution

Thermal behavior of the dish structure is very critical. Dish temperature distribution is a rather random phenomenon depending on structure style, time, solar radiation and wind condition. For close backup structure, Greve[7] did a number of measurements on IRAM 30 m telescope with the temperature control system not working. The vertical gradient within the backup structure varies from - 0.4 to +1.1 degrees. The horizon temperature gradient varies from + 0.2 to + 2.4 degrees(from Figs. 4.14 and 4.16 of reference [7]). This antenna has been well insulated. For antenna structure with sun shield on the back of the backup structure, Lamb and Forster did measurements on 6 m BIMA antennas[14], when the ventilation fan is not working, the measured temperature difference between front and back of the backup structure ranges from - 2.5 to + 2.5 degrees and the horizontal temperature difference ranges from -2.3 to + 1.7 degrees(it could be occasionally from - 4.5 to + 6.0

degrees). For indoor open backup structure, Bregman and Casse[12] also predicted a 0.9 degrees difference between bottom and top of the backup structure. However, for antennas with completely open backup structure, practical data is not found yet.

For an open backup structure, temperature differences between various components of the dish surely exist. Since the panels are under the solar radiation during the day and most of the backup structure members are in the shadow, the panel temperature will be higher than that of the backup structure. A Nastran model has been provided for a horizontally placed aluminum panel of 1 m size under the sun. Figure 10 shows this model. The convection coefficients of the front and back sides are calculated from the previous formula, being 3.6 W/m^2K for the front surface(face up) and 1.0 W/m^2K for the back surfaceface down). Since the panels on the backup structure are tilted, the convection coefficients will be larger than calculated. Taking the following conditions as: front air temperature is 20 C, rear air temperature is 22 C, sky radiation temperature is 5 C, ground temperature is 25 C, the absorptivity of the panel is 0.1 and emissivity is 0.1, solar loading is1260 W / m^2, then the calculated panel temperature is 36 C which is 14 degrees higher than the air temperature. This number is close to the measured data from BIMA antenna which is about 10 degrees higher than air temperature(note, a lower convection coefficient has been used here). Aluminum panels have good conductivity, the temperature gradient within the panels are small. However, for honeycomb panels, thermal gradients will be built up within the panel and will cause surface distorsion.

Within an open backup structure, if the backup structure is made of nearly uniform thin wall tubes, their time constant is easy to calculate. For CFRP tubes, taking the tube dimension D as 0.03 m, the natural convection coefficient calculated for the tube is 20.4 W/m2K. If the tube has its wall thickness being 0.003 m, the time constant is 1600x710x0.003/20.4 =170 sec. The time constant being 3 minutes is less than the change rate of the average air temperature, therefore the backup structure should have their temperature being the same as air temperature unless the sun is directly on the tubes. The tube time constant is proportional to its wall thickness, thick wall tubes have to be avoid in the design of the backup structure. This is also true for box type backup structure with large openings. The tube temperature under the solar loading will be discussed in the following paragraph.

For open backup structure, some structure members may be exposed to solar radiation during day time while other members are in the shadow of the surface panels, this brings uneven thermal expansion and is the reason for the backup structure deformation. For backup structure members of 1 meter in length, if the temperature difference between members is 10 C, then the distortion of the structure will reach 0-40 microns even it is made by CFRP material. The steel joints also bring significant thermal expansion to the backup structure. To reduce this distortion, it is necessary to lower the temperature difference. For evaluating the temperature caused by solar radiation, a Nastran heat transfer model has been produced. The model is shown in Figure 11. The model is a half tube, it involves 18 shell elements. The diameter of the tube is 25 mm and the wall thickness of

the tube is 3 mm. The solar radiation comes from one direction and the tube is also interacting via radiation with sky and via convection with the surrounding air. Tubes with different materials, different absorptivity and emissivity have been calculated. In the calculation, the ambient air temperature used is 25 C and the sky temperature is 10 C. The Nastran analysis shows the temperature of each grid point. The results are shown in Table 7.

Table 7 Temperature of tubes under direct solar radiation

tube material	convection coefficient	surface absorptivity	surface emissivity	tube high temperature	tube low temperature
steel	7.5	0.8	0.8	45.3	44.3
steel	7.5	0.3	0.8	29.5	29.1
steel	0.0	0.8	0.8	67.6	66.6
steel	20*	0.1	0.1	27.0	26.9
CFRP	7.5	0.8	0.8	50.6	40.0
CFRP	7.5	0.3	0.8	31.5	27.5
CFRP	20	0.1	0.1	27.6	26.4
CFRP**	20	0.1	0.1	26.3	25.7
CFRP	20	0.04	0.04	25.5	25.3

* the calculated nature convection coefficient for 1 inch tube is 20 W/m^2K.

** The solar loading is half of 1260 W/m^2 in this case.

From the calculation, it can be found that with absorptivity and emissivity as high as 0.8, the steel or CFRP tubes may have their temperature 20 C higher than that of the ambient air. The CFRP tube has larger temperature difference between front and rear surfaces. For tubes with some coating, the resulting temperature will be much lower. If the absorptivity and emissivity of the surface of the tubes are 0.1, then the temperature for steel or CFRP tubes is only 27 C, it is just 2 C higher than the air temperature. At this time, CFRP tube has a 0.8 C temperature difference within the tube and the steel one has only a 0.1 C difference. If the tube surface are reflecting gold(there is gold tape available which can be used to protecting CFRP tubes), the absorptivity and emissivity could be even lower. In this case the temperature increase of the tube will be less than 1 C. If the tube has its absorptivity and emissivity being 0.04, the temperature of the CFRP tube is only 0.5 C higher than the ambient air. In Table 7, the natural convection coefficients used are two numbers, one is 7.5 W/m^2K, and the other is 20 W/m^2K. The smaller one is for plate structure and the later one is for tubular structure. The tubulare data is calculatedfrom the

previous formula. The tube has a larger convection coeefficient, since its shape makes it easier to form a laminate flow around its surfasce. From the same table, it also shows that when the radiation received by the tube is halved then the temperature increase will reduce (nearly half) as well.

2.5 Dish distortion caused by temperature gradient of the backup structure

In general, three patterns of backup structure temperature gradient are common for millimeter antennas(note, most millimeter antennas have enclosures, insulations or sun shields outside their backup structure). These are: front to back gradient; radial gradient from the center towards the edge and temperature gradient from one side of the dish towards another side. For closed backup structure or those with sun shields, these temperature gradients has been observed and recorded[13]. A gradient along the radial direction may be caused by larger mass distribution towards the dish axis or higher convection coefficient near the edge of the dish. A gradient between front and back members of the structure may be caused by the higher temperature of the reflecting panels. A gradient along the diameter is mostly when the antenna is pointing to horizon. All these three gradient patterns are shown in Figure 12. For open-air backup structure, these temperature pattern effect will exist but it may be much smaller since the air arround members is free to circulate. However, there may exist other local patterns due to the direct solar radiation.

For assessing the thermal gradient effect on the backup structure, Nastran analysis of these three cases has been performed. In the analysis, the thermal expansion effect of the steel joint nodes is also considered. The coefficient of thermal expansion used for the structure members with joint nodes is $2x10^{-6}C^{-1}$. If the joint nodes are made from invar, the calculated distortion will be smaller. In the Nastran analysis, the first case calculated is 1 C difference between front and back. The calculated rms distortion of the surface nodes is 7.02 microns for CFRP backup structure and it is 44.4 microns for steel backup structure. After applying the parabolic fitting program, the residual rms error reduces to 1.36 microns for CFRP structure and it reduces to 8.7 microns for steel structure. The contour maps of the surface shapes before and after fitting of a CFRP structure is shown in Figure 13.

For the case of 1.5 C temperature difference between center and edge of the dish, the rms deviation calculated before fitting is 10.4 microns for CFRP structure and 18.5 microns for steel structure. After applying the parabolic fitting, the rms value for CFRP reduces to 3.9 microns and for steel material it reduces to 11.9 microns. The contour maps of the case are shown in Figure 14.

For case of 2 C temperature difference from one side to the other side of the dish, the rms deviation before fitting is 15.4 microns for CFRP structure and is 15 microns for steel structure. After applying parabolic fitting, the rms deviation reduces to 1.57 microns for CFRP structure and reduces to 3.7 microns for steel one. The contour maps of this case are shown in Figure 15.

By comparing these thermal induced reflecting surface error with the error budget[14], the conclusion drawn from these Nastran analysis are:

1) Steel backup structure may be difficult in satisfying the mmA antenna requirement, as any temperature gradient(1-2 degrees) will produce substantial distortion(15-44 microns before fitting and 4-12 microns after best fitting) to the dish surface.

2) If steel members are used for the backup structure, then the peak temperature differece of the backup structure members should be kept within 0.25 C.

3) A CFRP backup structure could tolerate some temperature gradients. For gradients of 1 - 2 C, the rms distortion of the dish surface is 7 - 16 microns before fitting and it is 1.3 - 4 microns after parabolic fitting. If the temperature gradient change is slow, the surface error is well within the mmA surface error budget. But in this case, the position of secondary mirror needs adjustment to suit the new fitted parabolic surface.

4) Local or randon temperature gradients of the backup struture will cause local distorsions. The effect of local distorsion is reduced if the rms error is concerned. The structure may tolerate slightly large local gradients.

5) If CFRP members and steel joints are used for the backup structure, the allowable temperature gradients should be arround 2 - 3 C. Without steel joints, the gradient tolerated can be 3-5 C..The gradients along radii cause larger distorsion than those in other directions.

6) Small temperature gradient of the backup structure causes reduction in antenna efficiency. Large temperature gradient may affect pointing accuracy as the best fitted parabola is away from the original parabola.

2.6 Thermal effect of tripod

Different from the thermal effect of the backup structure, the thermal effect of tripod concerns only the radiation pattern and the antenna pointing accuracy. When some members of the tripod structure have a higher temperature than the rest members of the tripod, the secondary morror position will undergo laterly displacement and tilt. This secondary mirror movement would then cause pattern degraderation and pointing error. For small movement of the secondary mirror, the resulted pattern effect is also called 'coma' effect. Baranne[15] gave the formula of the coma effect if the transverse decentering of the secondary mirror is u and the tilt angle about center of curvature of secondary is v:

$$K_c = [\,3\,Q^2 / 8\,f\,](m-1)^2[b_2(m-1) - (m+1)]u + [\,3\,Q^2/ 4\,f\,](m+1)(m-1)^2 f_2 v$$

where $Q = 1/(2N)$, N is aperature number of the system, m is the magnification factor of the secondary mirror, f is the final focal length, b_2 is the aspheric constant of the secondary, $f_2 = r_2/2$ and r_2 is the central radius of the secondary mirror. From this formula, it can be found that the coma effect by lateral displacement could be compensated by tilting the

secondary mirror in a proper direction. The servo control system of the antenna will provide the conpensation for the secondary mirror misalignment if it is small.

The second effect of the lateral movement is the pointing error. From geometry optical point of view, if the secondary mirror has a lateral moment u, then the image will have a corresponding movement which causes a pointing error of θ. The formula of this pointing error is given by:

$$\theta = (u / F_1) - (u / F)$$

where F_1 is the primary focal length and F is the system focal length. Taking $F_1 = 3.2$ m and $F = 96$ m, then a 0.05 mm secondary mirror lateral movement will cause 3.1 arc sec pointing error. This lateral displacement corresponds nearly 10 degrees temperature difference between one side of the tripod and another side of it if the tripod is built by CFRP material. Of course, most of this pointing error is also possible to be compensated by servo system of the secondary mirror. However, if the tripod is built by steel members, the mmA antenna may be difficult to achieve a 1 arc sec pointing requirement as it is too sensitive to the temperature change.

2.7 The mmA antenna thermal design

The purpose of the thermal design for mmA antennas is to provide a stable operational conditions, mainly on surface accuracy and pointing accuracy, for the antenna. From the thermal point of view, the antenna structure includes only three parts: the dish, the tripod and the base structure. The dish part concerns the surface accuracy as well as the pointing accuracy, the tripod and the base structure concern the pointing accuracy only.

The preliminary thermal design of the antenna is as follows:

* highly reflecting panel surface with a micro grating angle to direct the solar heat away from the secondary mirror;
* defused surface may be considered as an alternative choice;
* panel size is within 1 x 1 x 0.01 m, this is limited by thermal distorsion caused by temperature gradient;
* cast aluminum panel is prefered as it develops small thermal gradient under solar radiation;
* CFRP honeycomb panels could be used if their CTE is near zero;
* CFRP tube truss and steel nodes protected with shiny foil or paint for the backup structure;
* CFRP members with shiny protection or paint and imbedded thermal sensors for tripod;

* CFRP thin wall box structure could be used with the same protection as backup structure if their surfaces have large opening;

* no sun shield or ventilation fans is prefered on the backup structure;

* servo controlled secondary mirror motion mechanism to compensate pointing error and coma;

* insulated base supporter structure with larger thermal time constant;

* imbedded thermal sensor on the base supporter for pointing correction;

* tilt meters on the azimuth bearing could be used for initial pointing calibration;

* inside base structure, if heat source is involved, local insulation and ventilation should be provided to avoid direct contacting heat source with the structure members;

* reciever cabin will be kept at constant temperature.

REFERENCES

[1] Simiu,E and Scanlan R.H., Wind effects on structures, 2nd edition, John Wiley & Sons, New York, 1986.

[2] Shabana, A.A., Theory of vibration, Springer-Verlag, New York, 1991.

[3] Makowski, Z.S., From 'Analysis, design and construction of double layer grids', Applied science publisher Ltd., London, 1981.

[4] Schiff, D., Dynamic analysis and failure modes of simple structures, John wiley & sons, New York, 1990.

[5] Troitsky, M.S., Stiffened plates, bending stability and vibrations, Elsevier scientific publishing company, Amsterdam, 1976.

[6] Davenport,A.G., J. Struct. Div., Proc. Amer. Soc. Civ. Eng., Vol. 86, pp 39, 1960.

[7]Greve, A., Thermal design and thermal behaviour of radio telescope structure, IRAM, France, 1992.

[8] Almgren, D.W., Thermal design requirements and thermal boundary conditions for the SAO sub-millimeter array, Memo. 53, 1991.

[9] Kreith, F. and Bohn, M.S., Principles of heat transfer, Harper & row, publishers, New York, 1986.

[10] Lamb, J.W., Thermal considerations for mmA antennas, mmA antenna memo No. 5, 1992.

[11] Gray, D.E., American Institue of physics handbook, third edition, McGraw-Hill, Inc., 1972.

[12] Bregman, J.D. and Casse, J.L., A simulation of the thermal behaviour of the UK-NL millimeter wave telescope, Intern. J. of Infr. and Milli. Wave, Vol. 6, pp25, 1985.

[13] Lamb, J.W. and Forster, J.R., Temperature measurements on BIMA 6-m antennas --

Part I: backing structure, mmA antenna memo., 1993.
[14] Lamb, J. W., Proposed surface error budget for mmA antennas, mmA antenna memo. No. 11 1993.
[15] Baranne, Applied Optics, Vol. 12, p1427.

FIGURE CAPTIONS

Figure 1 Magnifcation factor varies with frequency ratio.
Figure 2 Modified tripod structure for the antenna.
Figure 3 Box-type ESSCO made antenna.
Figure 4 Antenna backup structure made of hexagonal elements
Figure 5 Antenna backup structure made by three rings of boxes elements.
Figure 6 Picture of the scaled model made by Composte Optics, Inc.
Figure 7 A very coarse model of a box type backup structure for Nastran analysis.
Figure 8 Absolute deflection curve of the box type model under gravitation force along the axis.
Figure 9 Wind energy spectrum for different wind speeds.
Figure 10 The panel thermal condition under the solar radiation.
Figure 11 The heat transfer model of backup structure tube
Figure 12 Three temperature gradients of backup structure
Figure 13 The distortion contour before and after fitting for case 1
Figure 14 The distortion contour before and after fitting for case 2
Figure 15 The distortion contour before and after fitting for case 3

TABLE CAPTIONS

Table 1 Vibration mode of the slanted-axis antenna
Table 2 Antenna natural frequency ratio and truss member size
Table 3 EAM as a function of elevation angle for a high altitude site
Table 4 Thermal properties of some structural materials
Table 5 Thermal properties of dry air at atmospheric pressure
Table 6 Absorptivity and emissivity of some surface materials
Table 7 Temperature of tubes under direct solar radiation

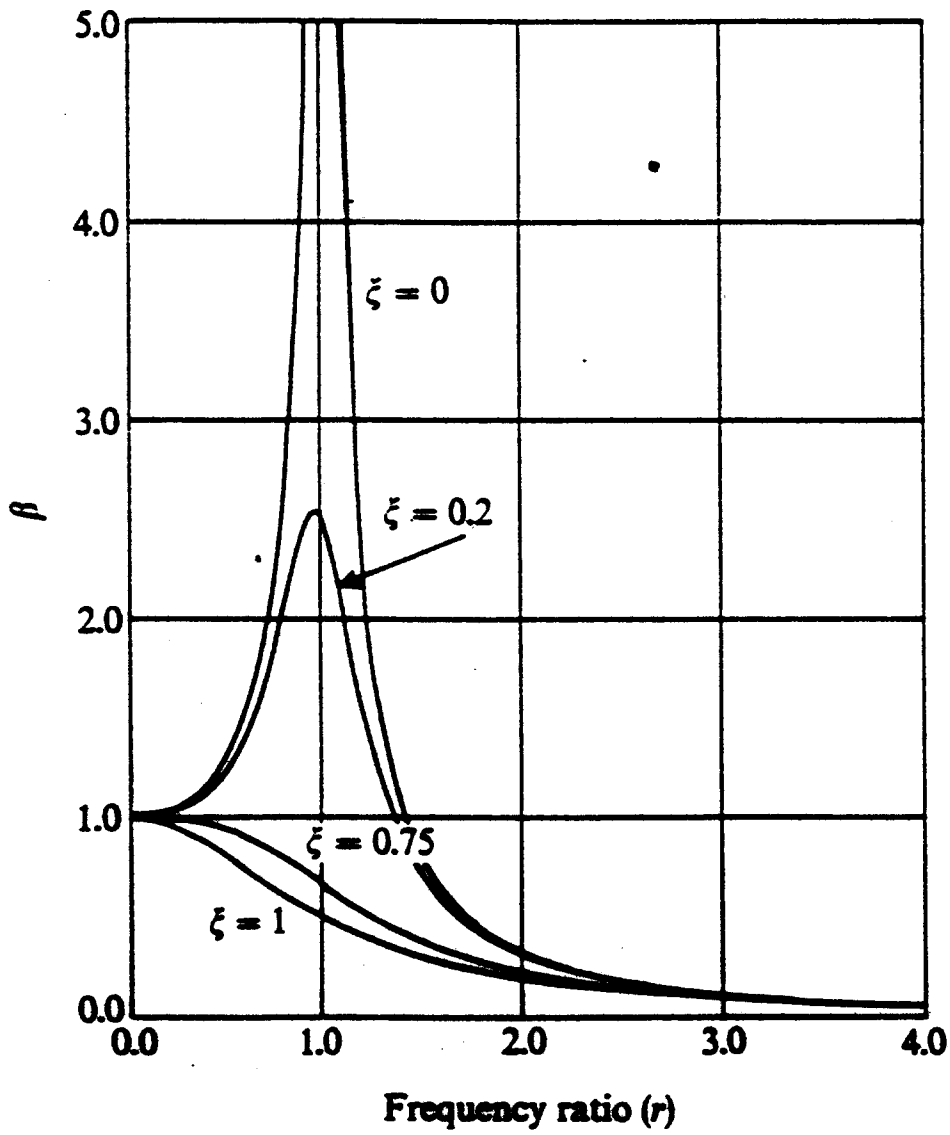

Figure 1 Magnifcation factor varies with frequency ratio.

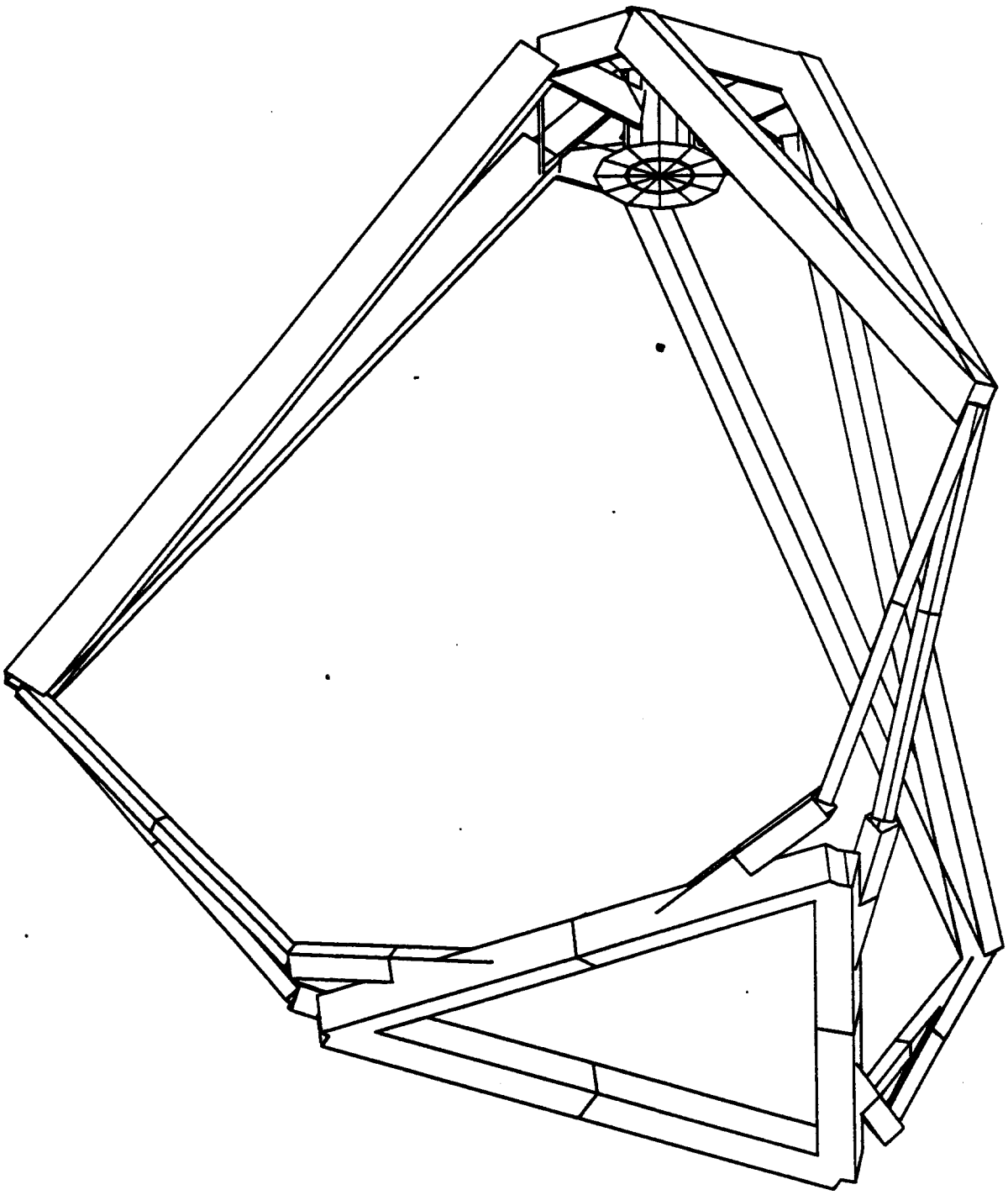

Figure 2 Modified tripod structure for the antenna.

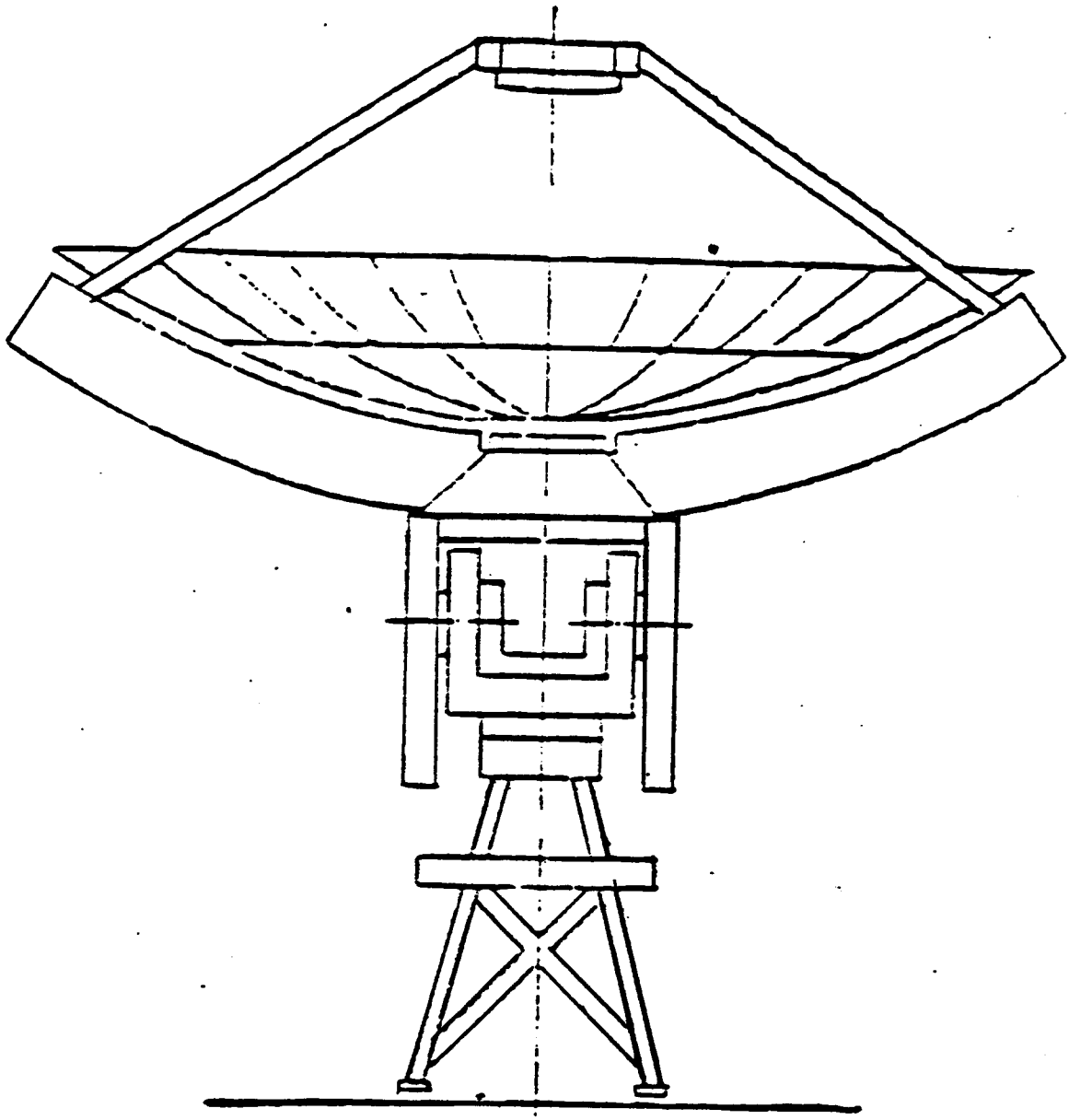

Figure 3 Box-type ESSCO made antenna.

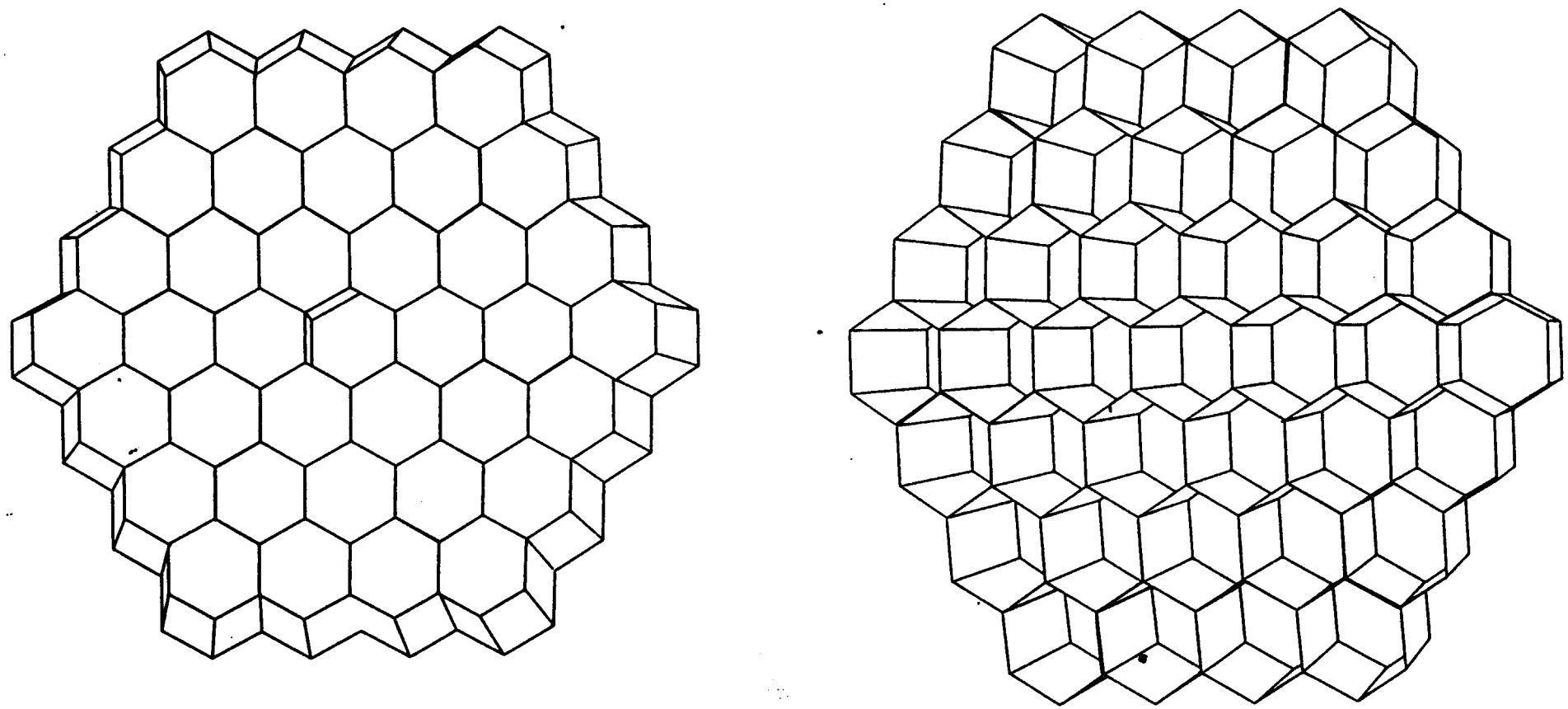

Figure 4 Antenna backup structure made of hexagonal elements

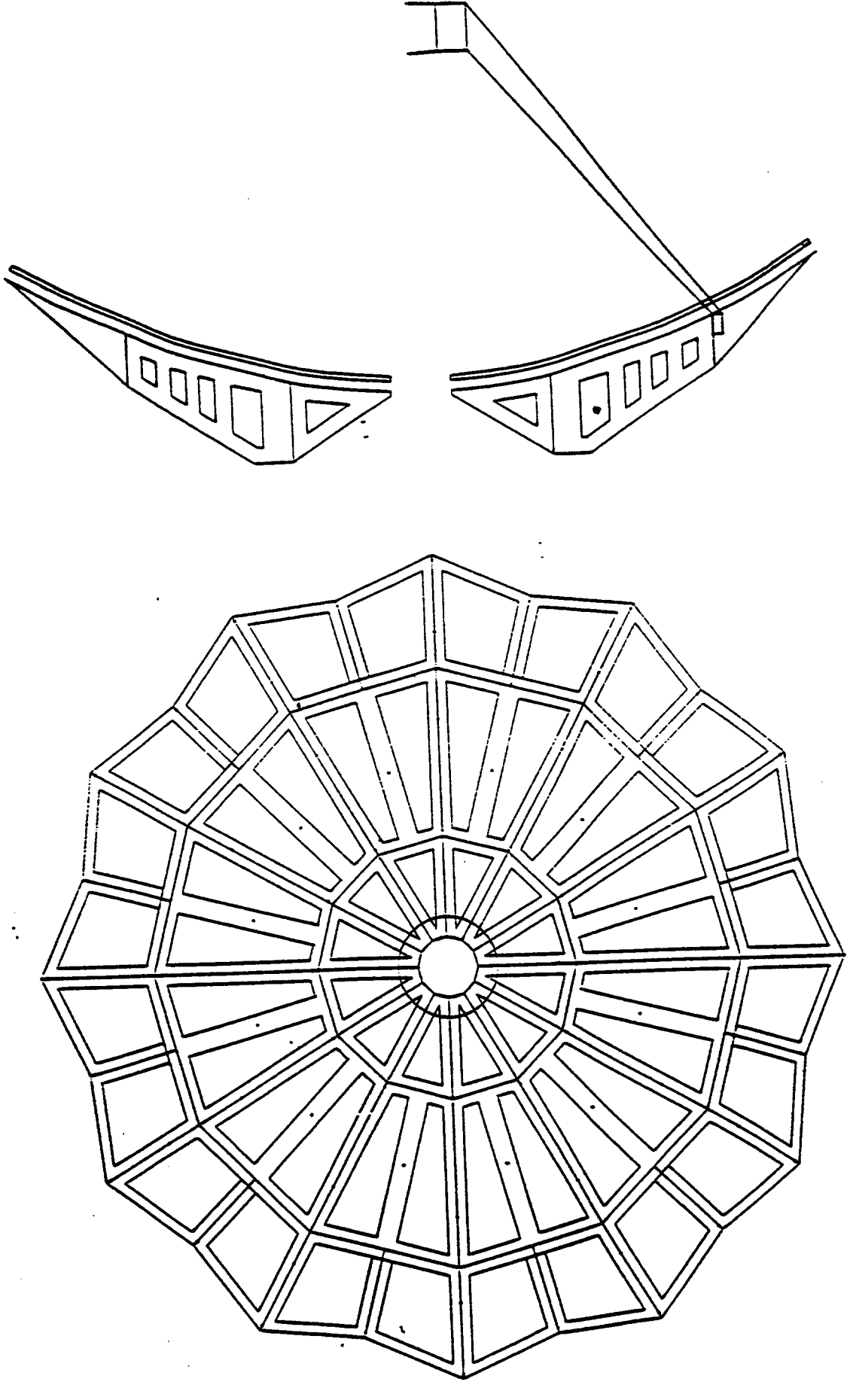

Figure 5 Antenna backup structure made by three rings of boxes elements.

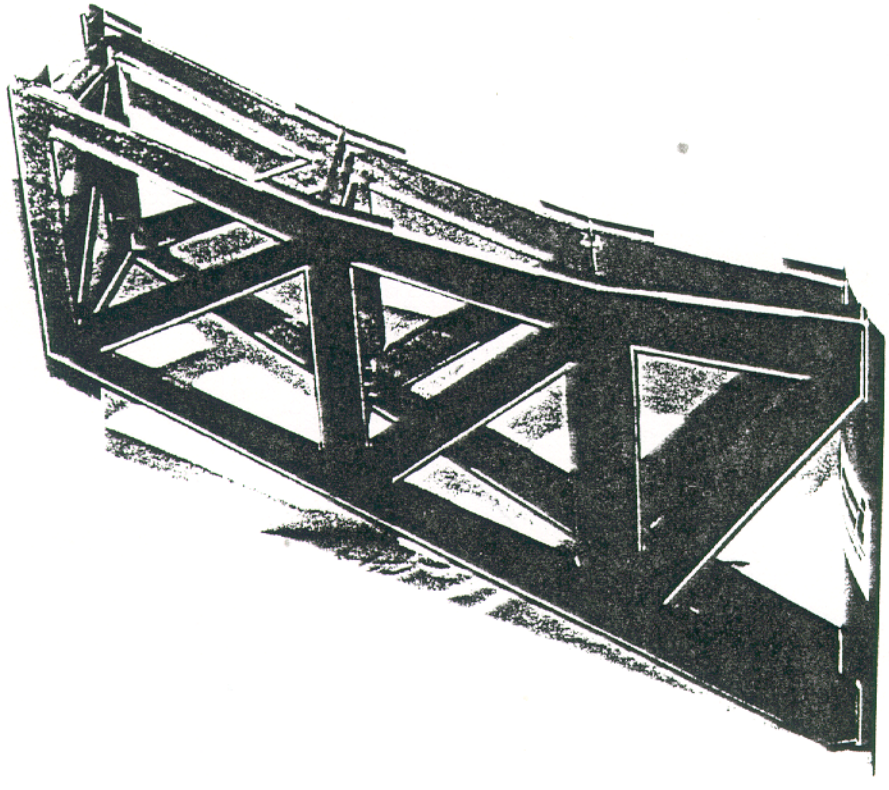

Figure 6 Picture of the scaled model made by Composte Optics, Inc.

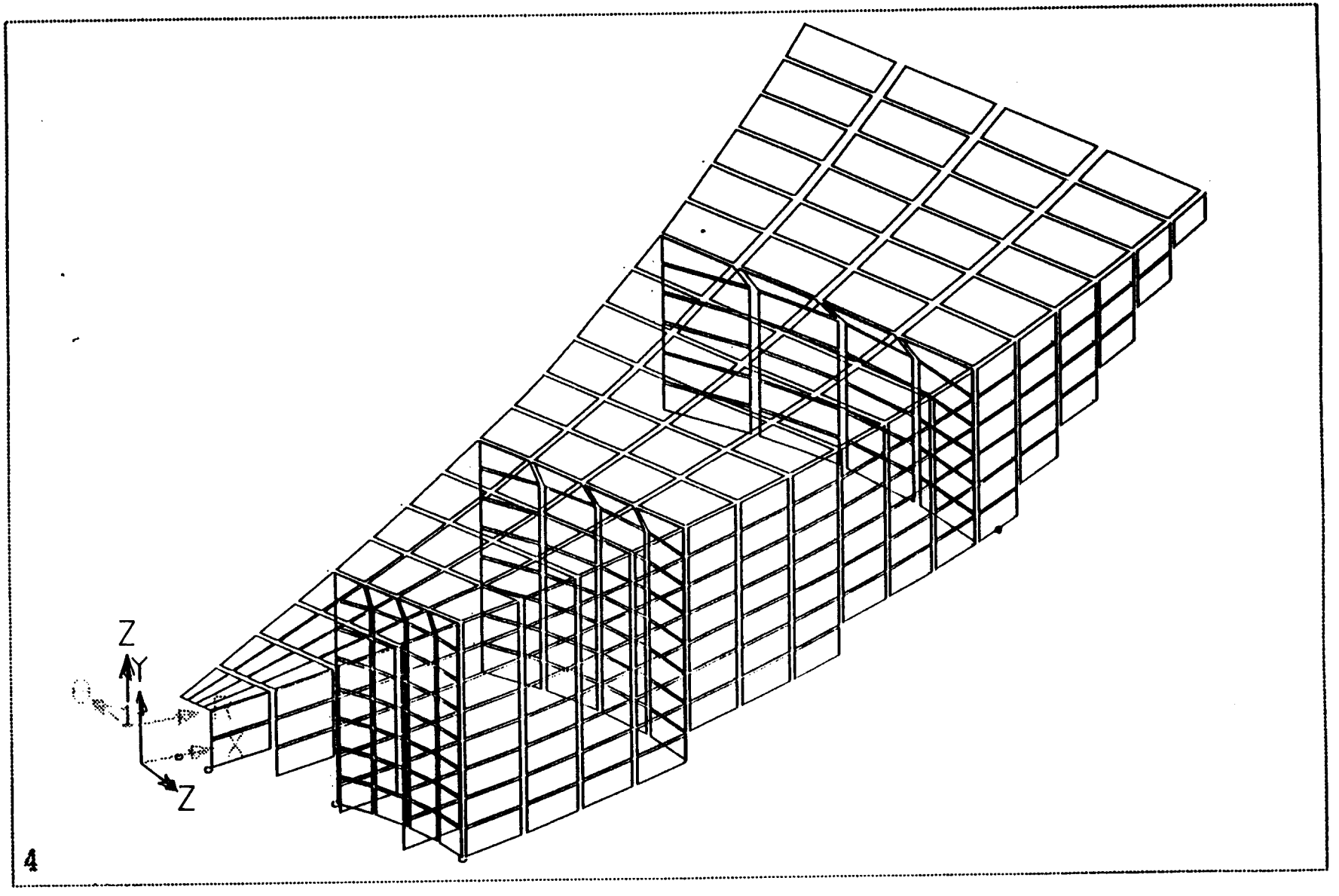

Figure 7 A very coarse model of a box type backup structure for Nastran analysis.

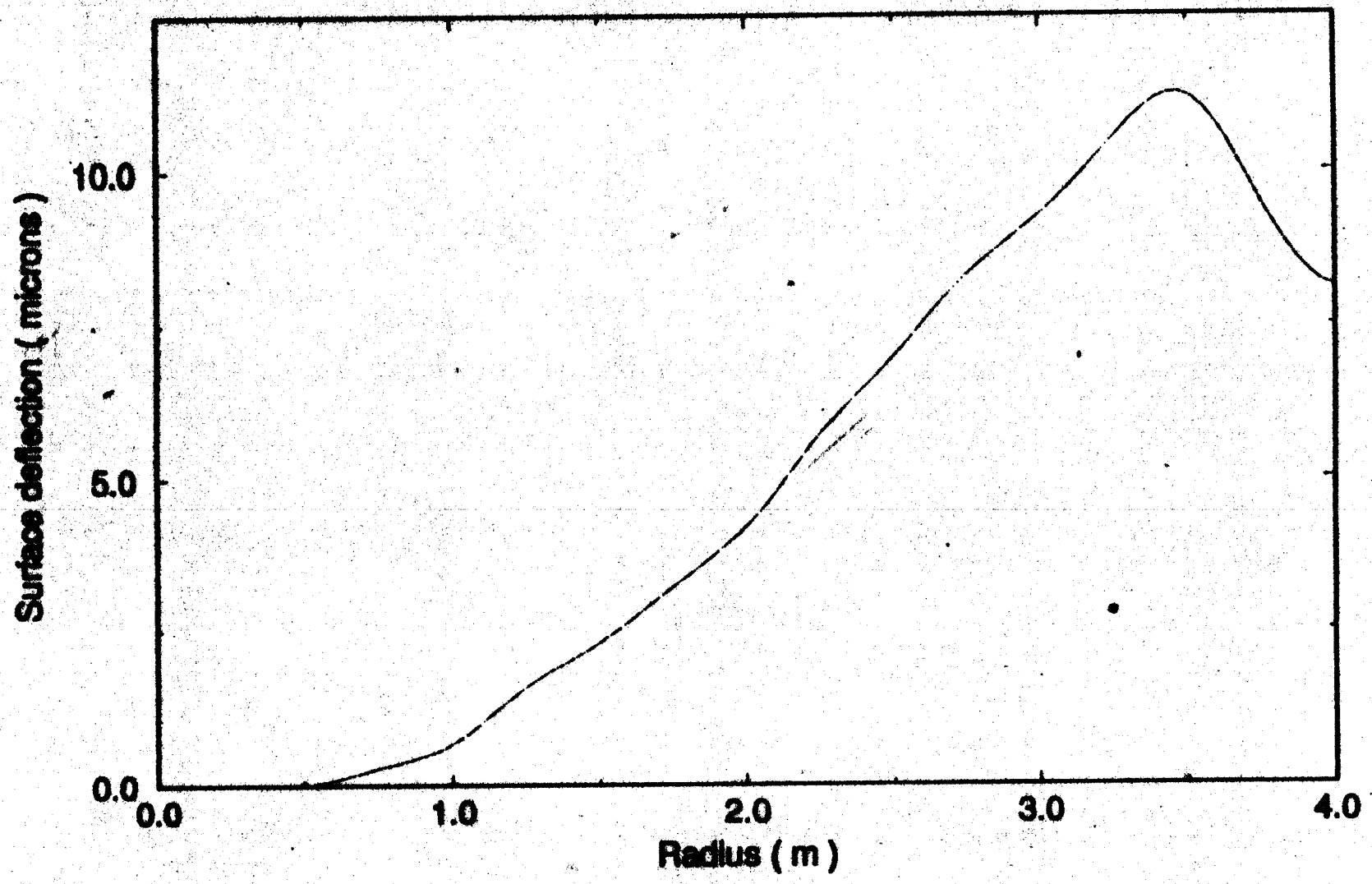

Figure 8 Absolute deflection curve of the box type model under gravitation force along the axis.

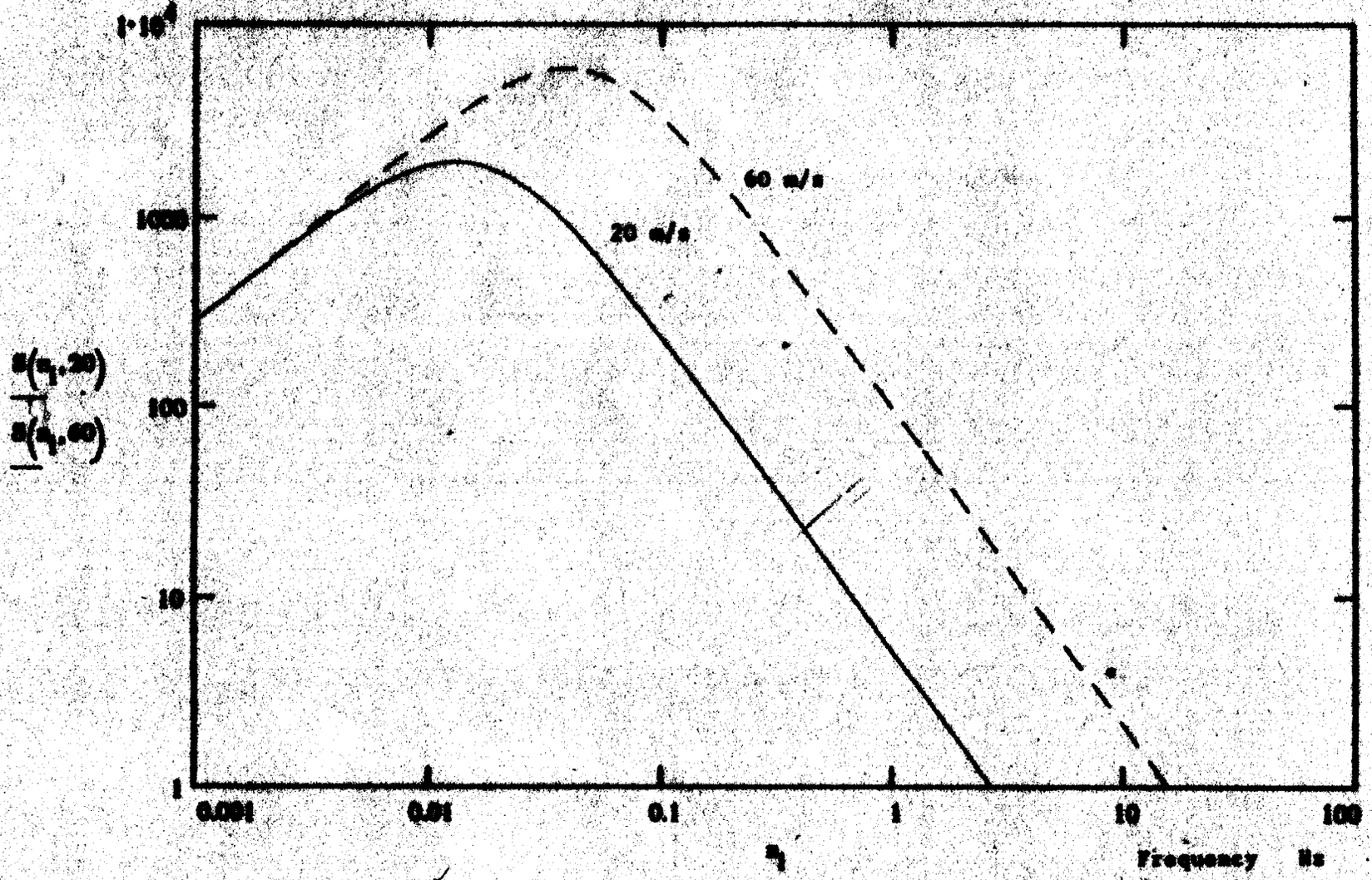

Figure 9 Wind energy spectrum for different wind speeds.

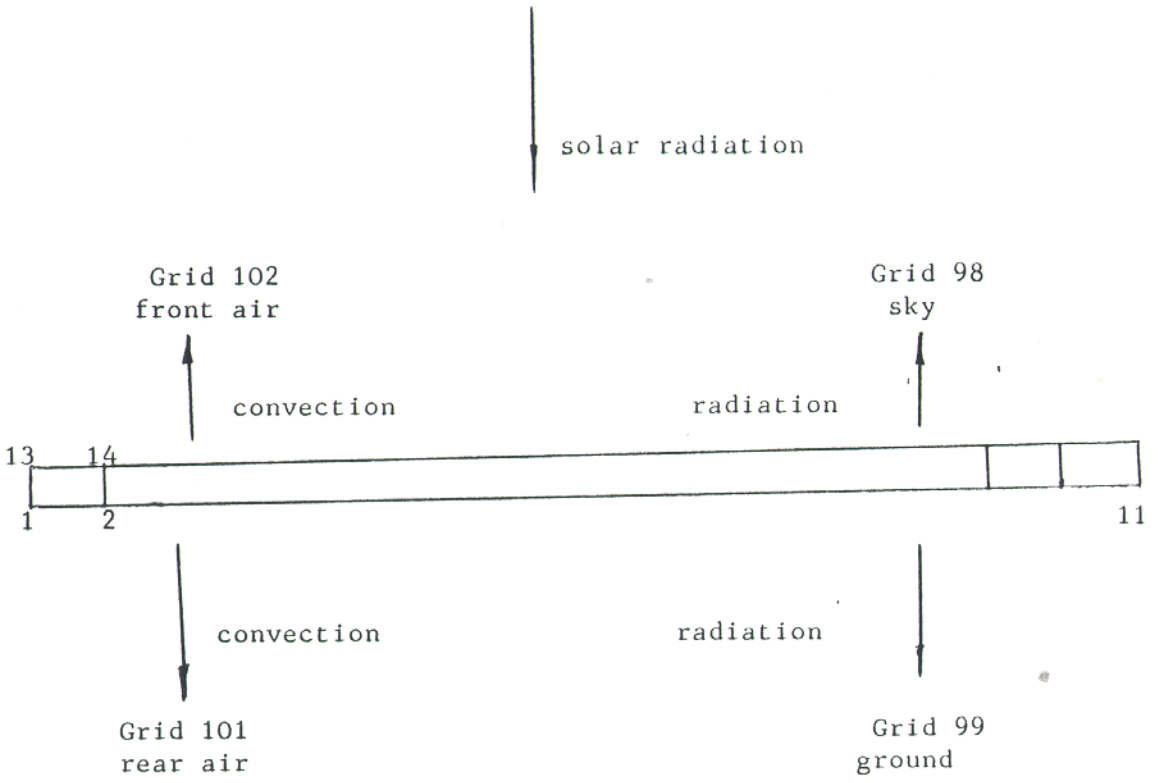

Figure 10 The panel thermal condition under the solar radiation.

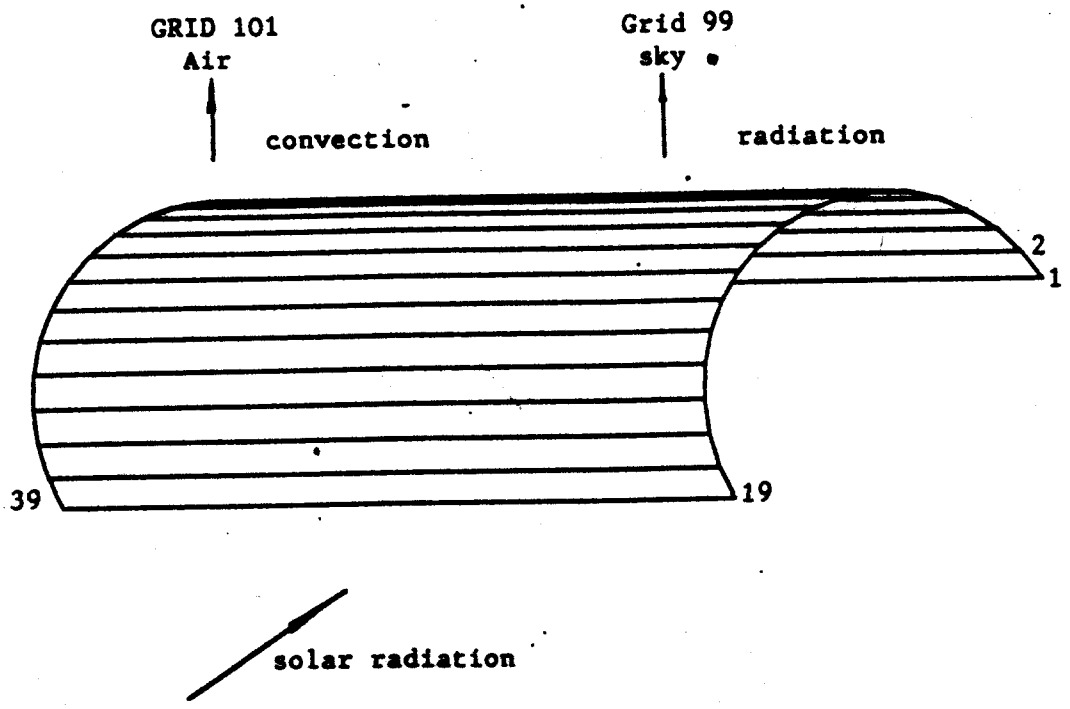

Figure 11 The heat transfer model of backup structure tube

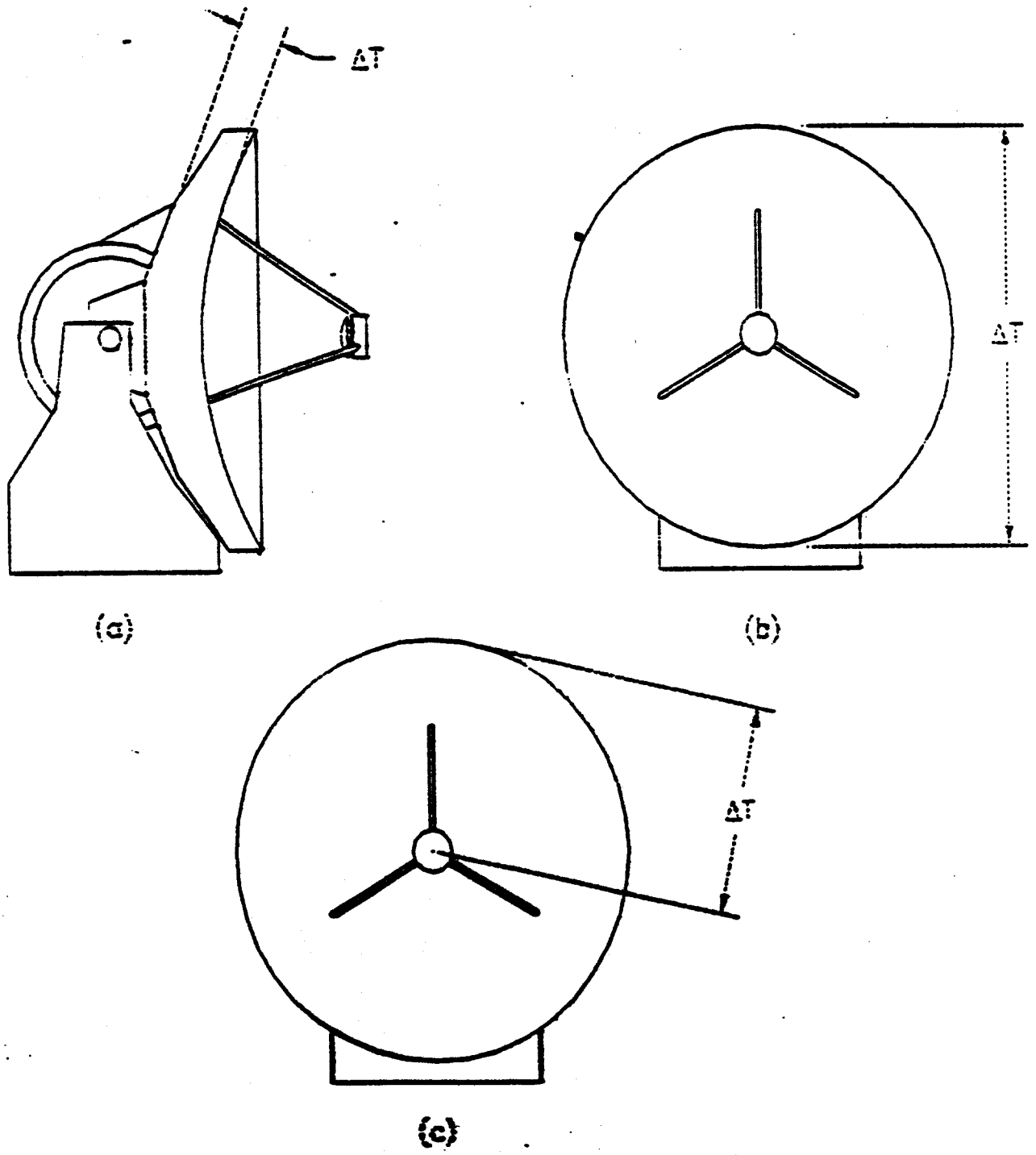

Figure 12 Three temperature gradients of backup structure

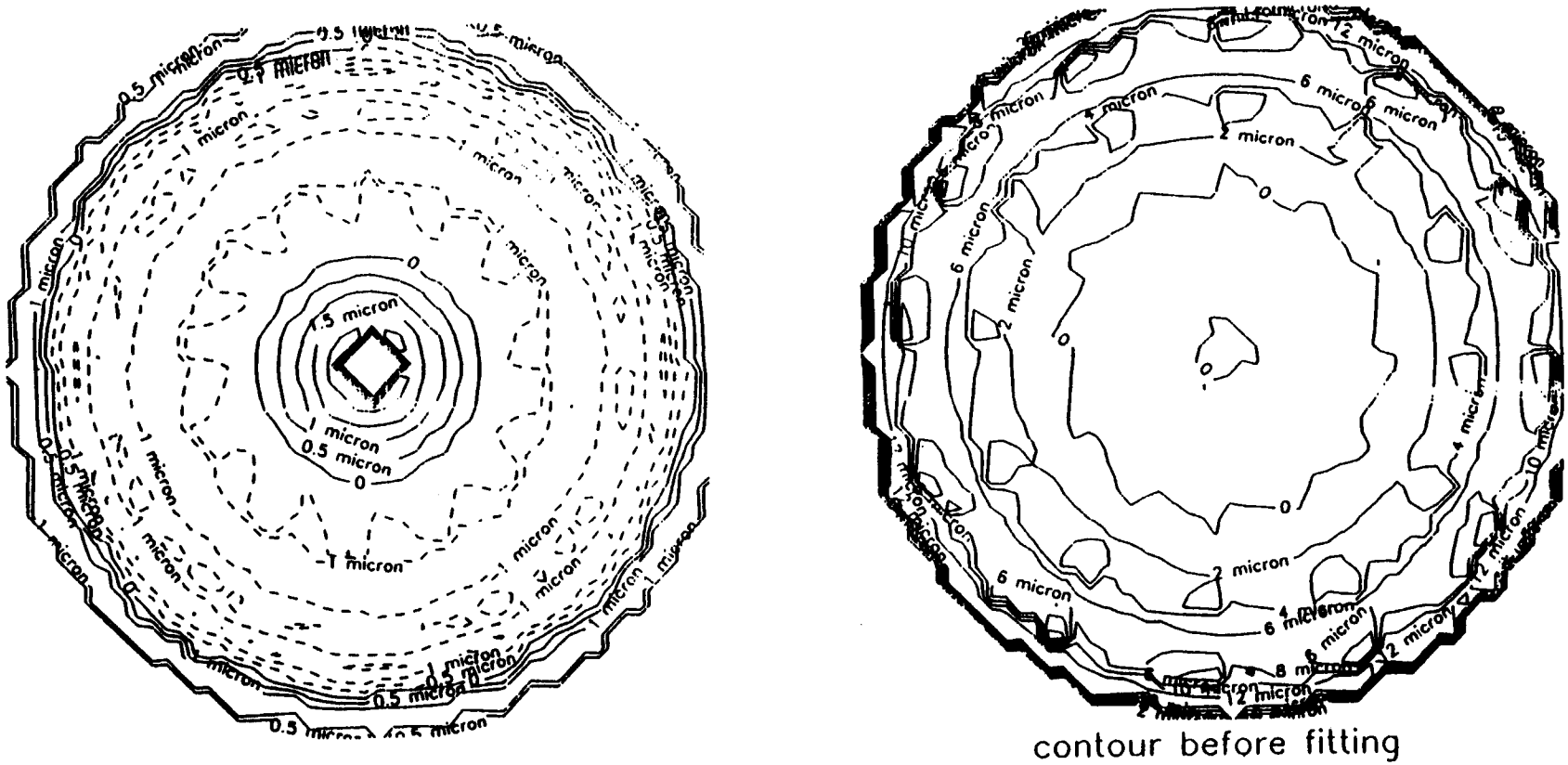

Figure 13 The distortion contour before and after fitting for case 1

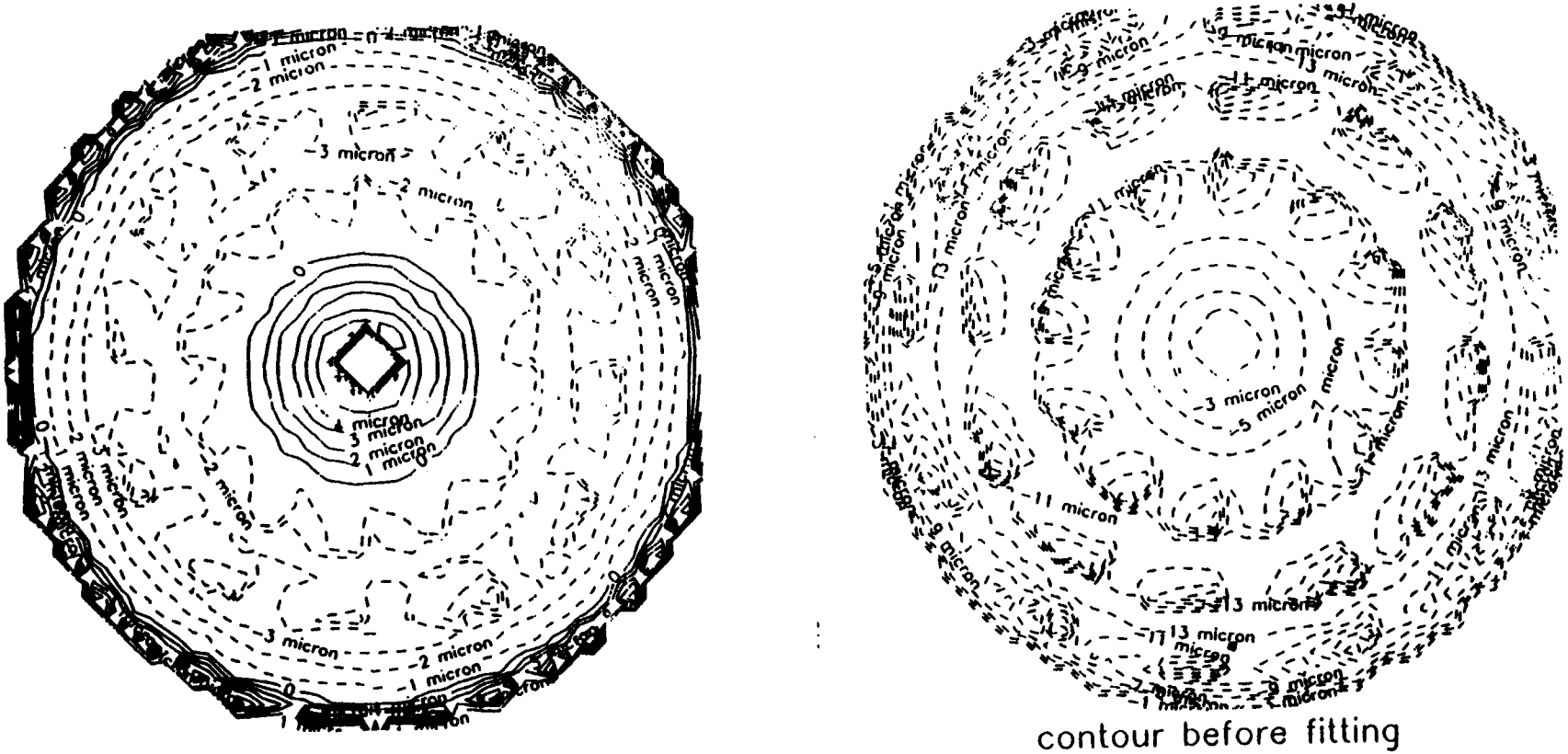

Figure 14 The distortion contour before and after fitting for case 2

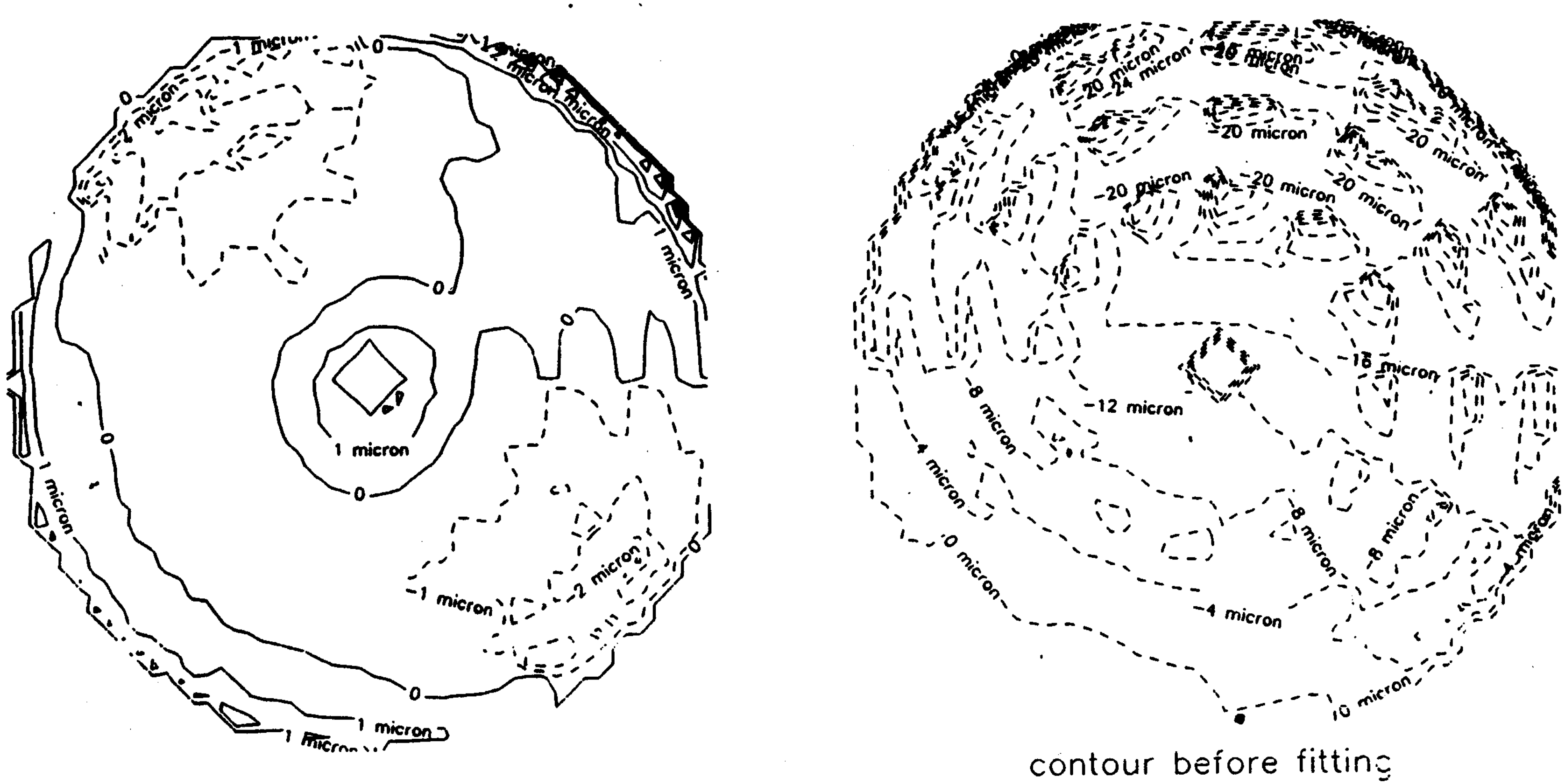

Figure 15 The distortion contour before and after fitting for case 3